

Electronic Supplementary Information

Low-cost smartphone-based Laser Induced Breakdown Spectroscopy (LIBS) combined with deep learning image processing for accurate lithology recognition

Xu Wang,^{‡ a} Sha Chen,^{‡ a} Mengfan Wu,^b Ruiqin Zheng,^a Zhuo Liu,^c Zhongjun Zhao^{*d} and Yixiang Duan

^{*a}

a. Research Centre of Analytical Instrumentation, School of Mechanical Engineering, Sichuan University, Chengdu, China, 610065, P. R. China.

b. College of Life Sciences, Key Laboratory of Bio-resource and Eco-environment, Ministry of Education, Sichuan University, Chengdu, China, 610065, P. R. China.

c. School of Aeronautics and Astronautics, Sichuan University, Chengdu, China, 610065, P. R. China.

d. College of Chemical Engineering, Sichuan University, Chengdu, China, 610065, P. R. China.

Corresponding Author

* E-mail: yduan@scu.edu.cn (Yixiang Duan); tompson_2006@163.com (Zhongjun Zhao)

Table of Contents

Experimental section

S1. Apparatus, spectral range, and wavelength calibration of SS	1
S2. Sample information, pre-treatment, and analysis	1
S3. experimental procedures of LIBS spectra acquirement by SS	1
S4. Single channel SS data of rock samples and the AES features in the spectroscopic images	2
S5. CNN model and implementation	2
S6. Comparison of lithological recognition results by different data sources and algorithms ..	2
S7. Intact rock samples analysis	3
Fig. S1	4
Fig. S2	5
Fig. S3	6
Fig. S4	7
Table S1	8
Table S2	10
Table S3	10

Experimental section

S1. Apparatus, spectral range, and wavelength calibration of SS

In the presented smartphone-based spectrometer, the grating is mounted behind the main camera of the smartphone (Galaxy S9+, Samsung), the optical path is covered by a 3D printed opaque chamber mounted to the back of smartphone. The collected emission light is introduced by an optical fibre with 200 μ m core diameter for single channel detection or a linear array of several fibres for multichannel detection, the entrance slit is not used considering to preserve larger input light amount for better sensitivity. The collected light was focused on the CMOS sensor by the own lens set of the smartphone, and the focus point was adjusted manually.

A mercury lamp (LTB Lasertechnik Berlin) was applied for evaluating the spectrum range and the resolution of the SS in this research. As shown in Fig 1 a, a long exposure image (2 seconds at ISO 100, aperture $f=1.6$) was captured by the single channel SS and was converted to the pixel number/wavelength-intensity form as the traditional spectrometer. The emission lines of Hg at 404.656nm, 435.834nm, 546.075nm, 576.961nm and 579.066nm could be observed clearly. linear regression of pixel numbers of emission lines appeared and the corresponding wavelength values was used for wavelength calibration and good linearity was obtained. As the result indicated, the smartphone-based spectrometer composed in this research could response in the range from 400nm to 650nm. In the converted spectrum of mercury lamp, the Hg peak at 576.961nm and 579.066nm could be separated clearly, the resolution of this SS is approximately 0.6nm as the full width at half maximum (FWHM) of these two peaks indicated.

A multi-channel spectral light collector was also designed in this research. As shown in Scheme 1A, a linear array of 7 PMMA plastic fibres (500 μ m diameter, without coating) were used to collect the emission light. At the collecting end, fibres were aligned by a 3D-printed holder with 0.25mm space between each fibre and able to collect the emission light distribution information in the distance of 5 mm from the sample surface along the direction of plasma propagation. At the entrance of SS, the fibres were still aligned and the distance between is 2mm, in order to separate the images corresponding to different channels on the detector.

S2. Sample information, pre-treatment, and analysis

Part of the lithological samples used in this research were provided by Chengdu Aliben Science & Technology Co., Ltd, and the others were Chinese national reference material purchased from Reference Material Center of China. The information of sample lithological type, sample ID (Chinese national standard material ID or the product ID) and element concentration distribution of every sample are displayed in Table S1. Before analyzed by LIBS, every sample was finely powdered, weighed (about 1g) and compressed to form a tablet using a hydraulic machine at 10MPa.

S3. experimental apparatus and procedures of LIBS spectra acquirement by SS

A compact air-cooled flashlamp pumped Nd:YAG laser(1064nm, 10ns pulse width) was used in this research (Chengdu Aliben Science & Technology Co., Ltd, China), the output energy per pulse was 100mJ+-5mJ and not adjustable, the repetition rate was fixed at 1 Hz.

To capture the LIBS information excited by laser shots, long exposure time is necessary because that the smartphone was not synchronized with laser. The laser was turned on manually after the image capture started. As the compact laser used in this research works at 1 Hz repetition rate, the exposure time was set as 4 seconds to accumulate the emission light from 4 successive laser ablations, other exposure parameters kept constant (iso=200, f=1.5) under the “professional mode” of the smartphone camera control interface. The images were saved as DNG format, the colour and the lightness of collected pictures were not further processed.

S4. Single channel SS data of rock samples and the AES features in the spectroscopic images

The Spectroscopic images were collected as the procedure described above by the single channel SS, 5 typical spectroscopic images of rock samples from each type were shown in Fig 2. Like the traditional spectrometer, the images could be converted to the wavelength-intensity form, the row of pixels in the middle of the image were selected, and spectrum data were obtained according to the gray values of pixels and the corresponding wavelengths calibrated above. The emission lines of major elements of different samples could be observed both in the converted spectra and the raw images.

A bright orange line corresponding to the Na 1 lines at 588.9nm and 589.5nm (labelled in red frame 3 in Fig 2A and arrow 3 in Fig 2B) could be observed in the spectroscopic image of igneous rocks, also there are high peaks in the converted spectrum. However, due to the limitation of the resolution, these two peaks were not well dispersed with each other. Intense lines in red region which represent the Ca related atomic and molecular emission light could be observed in limestones, dolomites, and gypsum rocks. Mg emission lines at 516.73nm, 517.27nm, 518.36nm (red frame 2 in Fig 2A, arrow 2 in Fig 2B), as the main difference between limestone and dolomites, were observed in the images and the converted spectra of dolomites and some of the gypsum samples. Emission lines of other elements such as Ba (blue/green line in most of the images of dolomite samples labelled by red frame 1 Fig 2A and arrow 1 in Fig 2B) could also be recognized.

The spectra of the same samples obtained by commercial spectrometer (Avantes, Netherland, resolution better than 0.2nm, detectable wavelength ranged from 322nm to 788nm, acquiring spectra with a 2 μ s delay time after the laser shots) were presented in Fig 2C.

S5. CNN model and implementation

As shown in Scheme 1C, in this working system, spectroscopic image is inputted, and the network first processes it through three rounds of hidden layers, each round including a convolutional layer and a maxpooling layer. Subsequently, the data flow through 2 convolutional layers, and further move into a flatten layer, a dropout layer and 3 dense layers. The output layer contains five vectors corresponding to the probability that the images belong to five lithological types. According to the maximum value of these vectors, the image is defined from which kind of rock.

CNN framework was selected for exploring the relationship between the samples' lithological type and their spectroscopic images by utilizing functional API in Keras (version 2.2.5) based on Python (version 3.6.5). The CNN model was constructed using the “hold-out validation” strategy in purely supervised mode. The dataset was divided into three

different sub-datasets, including training set (26 samples), validation set (20 samples) and test set (20 samples). Each sub-dataset was independent and consisted of samples from different type of rocks.

S6. Comparison of lithological recognition results by different data sources and algorithms

To investigate the advantage of the additional dimension of plasma propagation related features collected by the multichannel SS, comparison of CNN recognition result obtained from multichannel and single channel spectroscopic images was carried out. The single channel data were obtained by cut out the first channel of the multichannel data. The results of the confusion matrix for test dataset of single channel data were shown in Fig S1.

The comparisons between the presented strategy and commonly accepted spectroscopical machine learning lithological classification methods (SVM was selected) were conducted too. The spectra of the same samples recorded by a commercial spectrometer were collected and analyzed, the spectrometer was purchased from Avantes, Netherland, the resolution is better than 0.2 nm in the range from 322nm to 788nm, the delay function was realized by a customized delay generator (Chengdu Aliben Science & Technology Co., Ltd) and the delay time between laser shot and data acquiring is set as 2 μ s. As the image acquiring procedure by SS, the same number of spectra (10 from each sample) were collected, each spectrum was accumulated from four laser shorts at one location on the sample surface. SVM model was constructed based on Radial Basis Function (RBF), the best parameter of cost (C) was 1 and gamma (γ) was 0.1 which were determined by grid search method, and the confusion matrix of test results was shown in Fig S2.

In addition, wavelength-intensity form spectra converted from the images obtained by the first channel of the SS were also analyzed by similar SVM method constructed based on Radial Basis Function (RBF). The best parameter of cost (C) was 0.1 and gamma (γ) was 0.1, and the confusion matrix of test results was shown in Fig S3.

S7. Intact rock samples analysis

Two intact rock samples were analyzed directly for further verify the practicality of the presented method. The fresh and flat section surfaces of rock samples were selected and shot by laser without any pre-treatment. The samples were also pre-treated by powdering and tableting for comparison. The samples were drilling core samples provided by Chengdu Aliben Science & Technology Co., Ltd., and the elemental concentrations of main components were determined by X-ray fluorescence method (PANalytical Axios, analyzed at the Analytical & Testing Centre of Southwest University of Science and Technology, according to the Chinese standard method JY/T 0569-2020: General rules for wavelength dispersive X-ray fluorescence spectrometry). The concentration information results of main components (wt%) were listed in Table S3. According to this table, these two samples could be recognized as limestones.

The photos and spectral images of these samples obtained by direct analysis and pre-treated samples were shown in Fig S4. Although the appearances of the samples changed significantly after the pre-treatment, the spectral images still presented almost the same features and even intensities.

Figures and tables:

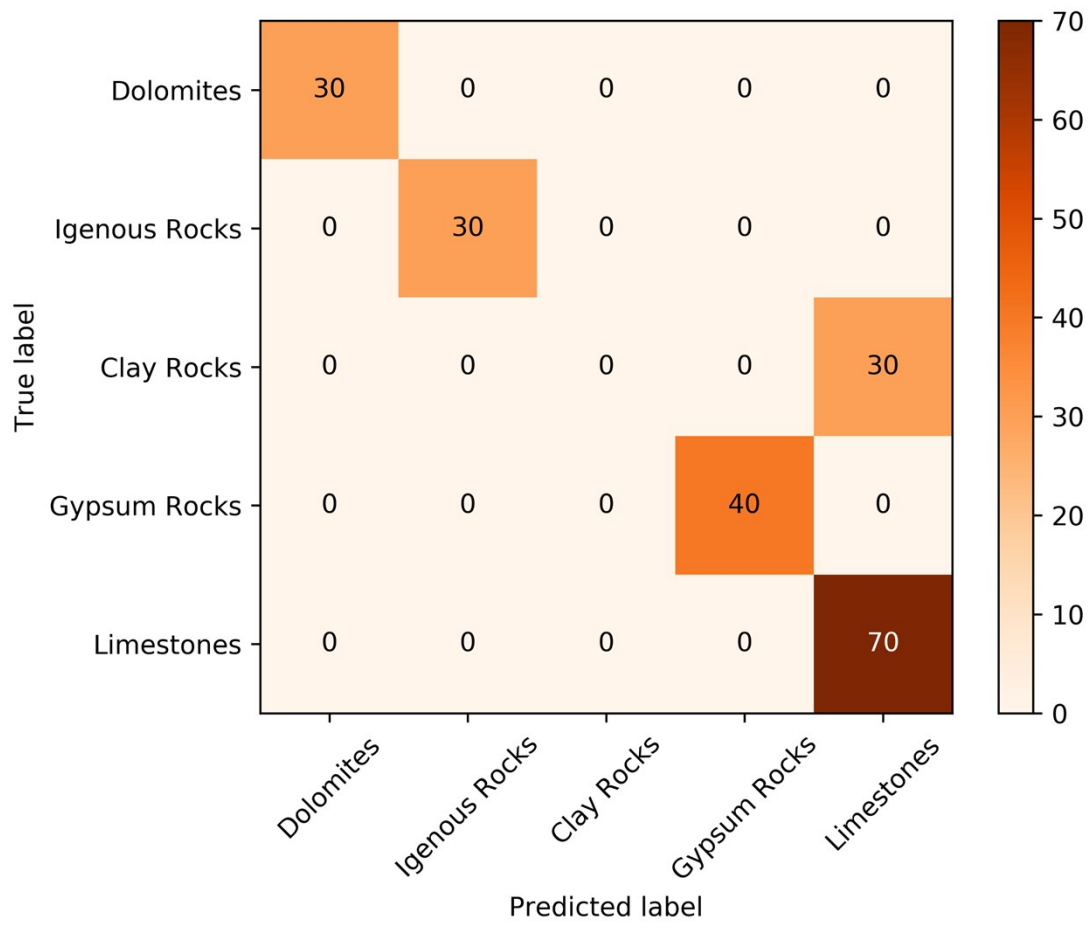


Fig. S1 Confusion matrix of test results based on the single channel data of SS in image format

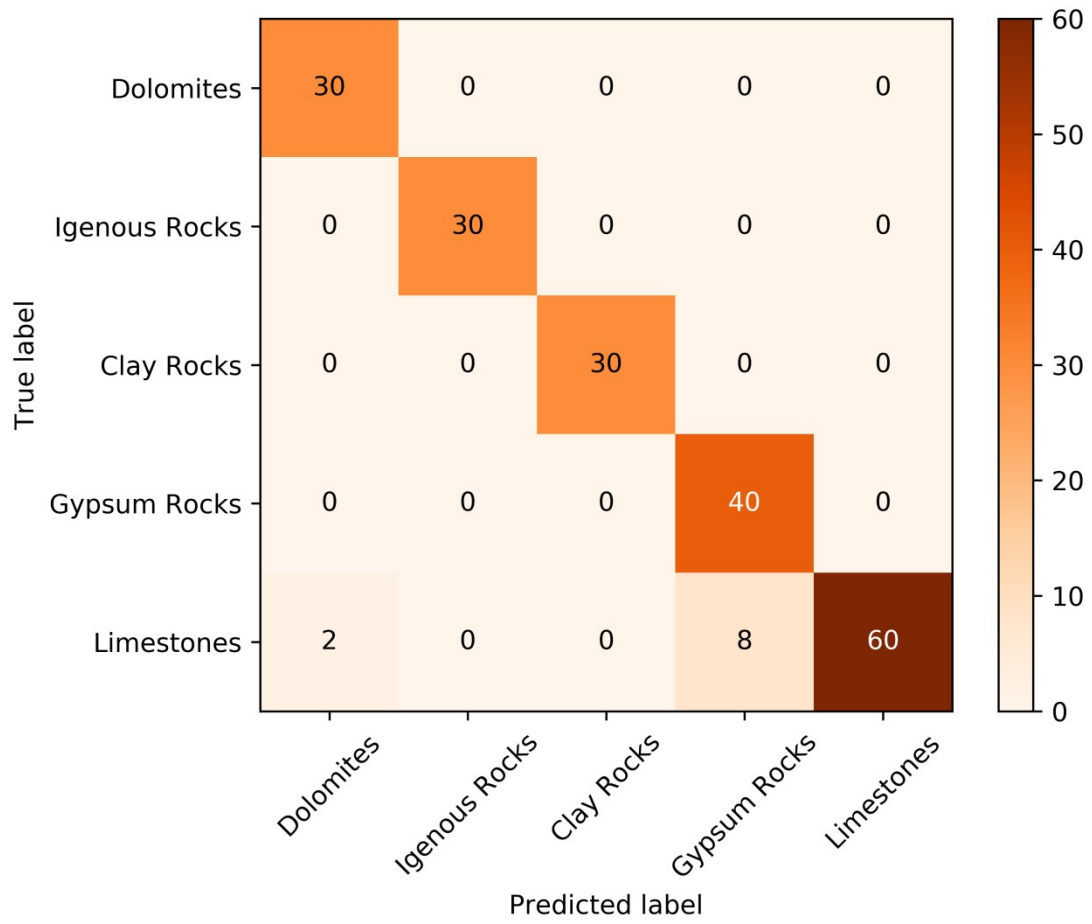


Fig. S2 Confusion matrix of test results based on the data collected by commercial spectrometer

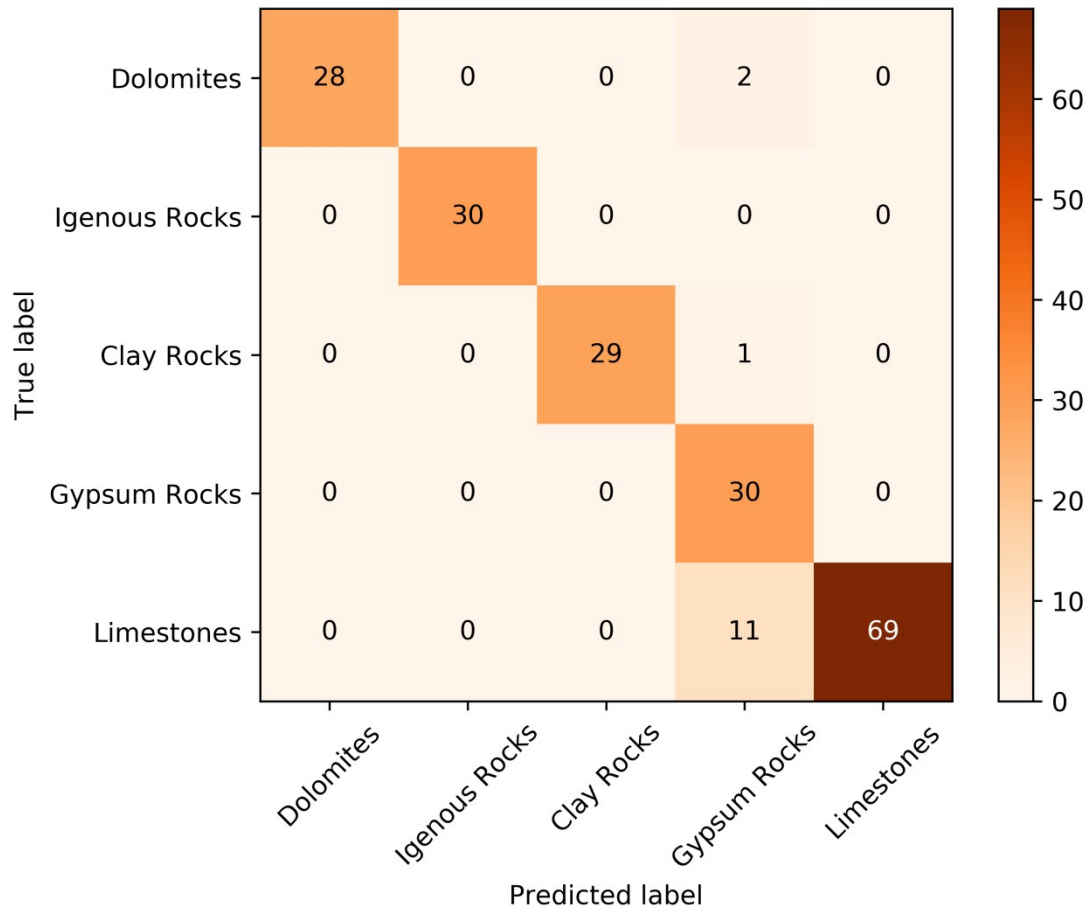


Fig. S3 Confusion matrix of test results based on spectra converted from channel 1 of SS

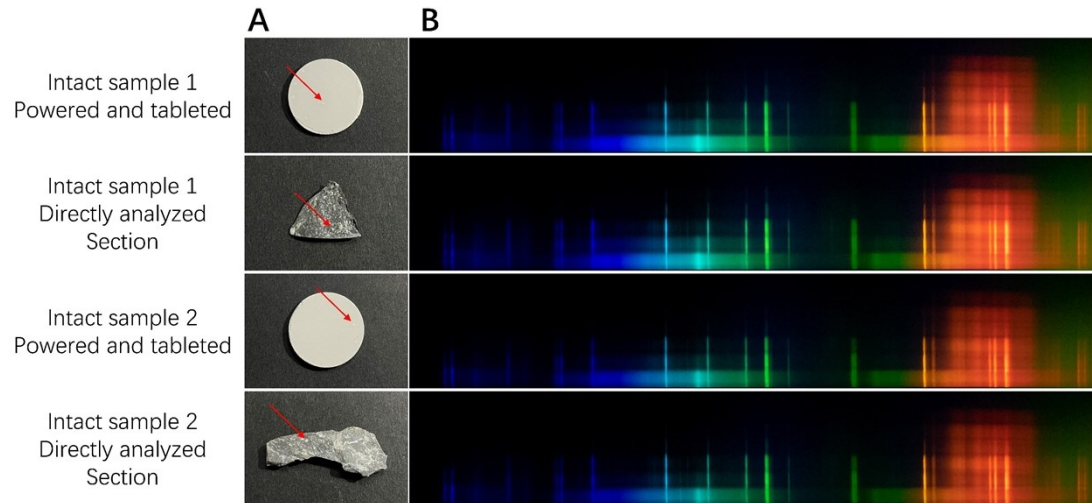


Fig. S4 (A) The photos of the section surfaces of the intact rock samples and the pre-treated sample tablets, the red arrows pointed to the laser ablation points, (B) the spectral images of the samples obtained by the SS-LIBS presented in this research.

Table S1 The information of all the 66 samples employed in the experiment. Every concentration value is expressed by weight percentage (in unit of %). In the column of Sample No., “T” indicates test sample, “*” indicates validation sample and others are training sample. In the column of Sample ID, “GBW” indicates the sample is from Reference Material Center of China, “ALB” indicates the sample is provided by Chengdu Aliben Science & Technology Co., Ltd.

Sample No.	Lithology	Sample ID	Fe	Ca	Mg	Ti	Na	Ba
D01*	Dolomite	GBW07114	0.028	21.4	13.1	0.009	0.0223	0.00443
D02	Dolomite	GBW07136	0.0399	23.6	10.8	0.0018	0.0193	0.00256
D03 ^T	Dolomite	GBW(E)070157	0.333	20.5	11.9	0.0216	0.0245	0.288
D04	Dolomite	GBW(E)070159	0.174	21.5	12.5	0.0072	0.00816	0.223
D05 ^T	Dolomite	GBW(E)070160	0.25	21.1	12.3	0.0126	0.0171	0.25
D06	Dolomite	ALB14749	0.321	26.9	9.23	-	0.0111	-
D07 ^T	Dolomite	ALB14750	0.347	25	10.7	-	0.00965	-
D08*	Dolomite	ALB14750a	0.188	22.8	12	0.011	0.0245	-
D09	Dolomite	ALB1575911	0.253	21	12.2	0.0144	0.0163	0.255
D10*	Dolomite	ALB15760	0.291	20.8	12.1	0.0171	0.0208	0.269
I01	Igneous Rock	GBW07103	2.29	1.11	0.252	0.172	2.32	0.0343
I02*	Igneous Rock	GBW07104	5.29	3.71	1.03	0.309	2.86	0.102
I03 ^T	Igneous Rock	GBW07105	15.3	6.29	4.66	1.42	2.51	0.0527
I04	Igneous Rock	GBW07109	5.18	0.993	0.39	0.288	5.31	0.0251
I05*	Igneous Rock	GBW07110	3.3	1.76	0.504	0.48	2.27	0.105
I06 ^T	Igneous Rock	GBW07111	4.24	3.37	1.69	0.462	3	0.19
I07	Igneous Rock	GBW07112	17.3	7.04	3.15	4.61	1.57	0.00862
I08*	Igneous Rock	GBW07113	2.24	0.421	0.096	0.18	1.91	0.0506
I09 ^T	Igneous Rock	GBW07121	3.43	1.9	0.978	0.18	3.93	0.114
I10	Igneous Rock	GBW07122	18.8	6.86	4.32	0.551	1.54	0.062
C01	Clay Rock	GBW03101a	7.39	0.0929	0.276	0.42	0.0445	-
C02*	Clay Rock	GBW03104	3.97	0.157	0.402	0.408	0.148	0.0402
C03	Clay Rock	GBW07107	5.32	0.429	1.21	0.395	0.26	0.045
C04 ^T	Clay Rock	GBW(E)070146	3.39	6.99	1.04	0.331	0.19	-
C05 ^T	Clay Rock	ALB0019	4.46	0.993	1.54	0.408	0.705	-
C06*	Clay Rock	ALB0038	2.2	3.17	1.18	1.78	0.468	1.92
C07	Clay Rock	ALB0039	2.57	4.16	1.57	1.95	0.495	2.37
C08 ^T	Clay Rock	ALB0086	5.14	1.67	1.24	2.91	0.73	1.85
C09*	Clay Rock	ALB0088	4.23	1.58	1.04	2.34	0.816	1.23
C10	Clay Rock	ALB0092	3.81	1.96	1.47	2.39	0.57	2.04
C11	Clay Rock	ALB0095	3.83	1.49	1.32	2.78	0.525	2.67
G01	Gypsum Rock	GBW03109	0.112	28	1.04	0.0096	0.0482	0.0003
G02	Gypsum Rock	GBW03111a	0.077	23.1	1.48	0.006	0.0104	0.00063

G03*	Gypsum Rock	ALB091111	0.0945	25.6	1.26	0.0078	0.0293	0.00046
G04 ^T	Gypsum Rock	ALB091112	0.0887	24.7	1.34	0.0072	0.023	0.00052
G05	Gypsum Rock	ALB091113	0.0858	24.3	1.37	0.0069	0.0198	0.00054
G06*	Gypsum Rock	ALB091121	0.1	26.4	1.19	0.0084	0.0356	0.00041
G07 ^T	Gypsum Rock	ALB091131	0.103	26.8	1.15	0.0087	0.0388	0.00038
G08*	Gypsum Rock	ALB0100	0.203	25	2.49	0.225	0.26	0.78
G09 ^T	Gypsum Rock	ALB0102	0.114	26.1	1.54	0.17	0.0764	0.581
G10	Gypsum Rock	ALB0106	0.0868	26.1	2.03	0.126	0.0393	0.976
G11*	Gypsum Rock	ALB0107	0.077	26.7	1.51	0.118	0.0586	0.556
G12 ^T	Gypsum Rock	ALB0108T	0.179	25	2.24	0.232	0.0905	0.507
G13*	Gypsum Rock	ALB0120	0.225	21.7	0.901	0.078	0.12	0.185
G14	Gypsum Rock	ALB0124	0.246	24.4	1.85	0.188	0.108	0.561
G15	Gypsum Rock	ALB0126	0.203	25.3	1.64	0.0979	0.0898	0.567
L01	Limestone	GBW03105a	0.077	38.6	0.486	0.006	0.0126	0.00111
L02*	Limestone	GBW03106a	0.119	36.9	1.35	0.009	0.0126	0.00271
L03 ^T	Limestone	GBW03107a	0.406	35.8	1.07	0.0312	0.02	0.0026
L04	Limestone	GBW03108a	0.266	33.6	3.49	0.018	0.0119	0.00176
L05 ^T	Limestone	GBW07108	3.04	25.5	3.11	0.196	0.0594	0.012
L06	Limestone	GBW07120	0.147	36.5	0.426	0.023	0.0223	0.0009
L07 ^T	Limestone	GBW07127	0.252	34.2	4.06	0.0066	0.0163	0.00097
L08*	Limestone	GBW07128	0.268	30	6.97	0.0132	0.0215	0.00116
L09*	Limestone	GBW07129	0.0544	39.6	0.144	0.0042	0.0104	0.0008
L10	Limestone	ALB303241	0.359	37.8	0.856	0.00336	0.0163	0.266
L11 ^T	Limestone	GBW(E)070147	0.175	33.4	3.93	0.0138	0.00816	0.00051
L12*	Limestone	GBW(E)070148	0.292	29.9	6.22	0.0186	0.00816	0.00074
L13 ^T	Limestone	GBW(E)070149	0.202	36.2	1.73	0.0192	0.0193	0.00194
L14	Limestone	GBW(E)070150	0.131	32.9	3.59	0.009	0.00742	0.0054
L15*	Limestone	GBW(E)070151	0.127	36.6	1.46	0.012	0.00549	0.00111
L16 ^T	Limestone	GBW(E)070152	0.106	38.4	0.702	0.0084	0.0043	0.00059
L17	Limestone	GBWE070153	0.211	34.7	2.59	0.0306	0.0208	0.0013
L18*	Limestone	GBW(E)070154	0.207	37.1	0.738	0.0216	0.00668	0.00232
L19 ^T	Limestone	GBW(E)070155	0.102	38.7	0.492	0.0096	0.00445	0.00068
L20	Limestone	GBW(E)070156	0.1	38.4	0.9	0.0066	0.00445	0.00068

Table S2 Comparison of test accuracy obtained by different data sources and algorithms/models

Input	Spectral range	Experimental apparatus	Methods	Test accuracy
Multichannel Spectroscopic images	400~650nm	SS in this research	CNN	100%
Single channel Spectroscopic images	400~650nm	SS in this research	CNN	85%
Spectra converted from channel1 of SS	400~650nm	SS in this research	SVM	93%
Spectra data	322~788nm	Commercial Spectrometer	SVM	95%

Table S3 The elemental concentration information of intact rock samples employed in the experiment

Compositions	Sample 1(%)	Sample 2(%)
SiO ₂	1.043	0.995
Al ₂ O ₃	0.305	0.248
Fe ₂ O ₃	0.146	0.116
MgO	0.317	0.314
CaO	53.300	53.368
Na ₂ O	0.056	0.060
K ₂ O	0.092	0.068
TiO ₂	0.018	0.013
MnO	0.003	0.003
P ₂ O ₅	0.011	0.009
SO ₃	0.355	0.294
Loss on ignition	42.311	42.535